

# Distributed control of coupled inhomogeneous diffusion in tokamak plasmas

Bojan Mavkov, Emmanuel Witrant, Christophe Prieur  
Univ. Grenoble Alpes, CNRS, GIPSA-lab, F-38000 Grenoble, France

**Abstract**—This paper proposes novel distributed control methods for the coupled dynamics of the safety factor and electron temperature profiles in tokamaks. The feedback design is based on an infinite dimensional setting using Lyapunov analysis for partial differential equations. The coupled dynamics is modeled by two 1D linearized resistive diffusion equations. We first propose a combined control of both dynamics based on stability analysis. A composite control is then synthesized using singular perturbation theory where the fast component of the electron temperature is decoupled from the slow component induced by the magnetic field dynamics. Both control methods are evaluated using the RAPTOR simulator and applied to the ITER tokamak device. The distributed control is performed using antennas operated at electron cyclotron frequency.

**Index Terms**—Distributed control methods, controlled thermonuclear fusion, Tokamak devices, partial differential equations, singular perturbation theory.

## I. INTRODUCTION

Tokamaks are large devices using a magnetic field to confine a hot plasma in the shape of a torus. Tokamak research aims at building a reliable power production system using controlled thermonuclear fusion [30]. Heating of the plasma comes from the electric currents obtained from several sources. The main source of current in a tokamak is the one induced by the transformer action caused by the central ohmic coil. Other sources of current are neutral-beam injection and radio-frequency (RF) antennas. There are several plasma parameters, such as the safety factor  $q$  (related to the magnetic flux) and the temperature of the electrons  $T_e$  that are defining the plasma state. Achieving a long term steady-state fusion reaction relies on advanced tokamak operation scenarios in which the profiles of  $q$  and  $T_e$  are optimized.

Simultaneous control of multiple plasma parameters profiles is a challenge, in particular because of the coupling between the magnetic flux and the pressure profiles. The safety factor is crucial to analyze magnetohydrodynamics stability and performance. The plasma resistivity, which governs the evolution of  $q$  [26], depends primarily on  $T_e$ . The dynamics of  $q$  and  $T_e$  are thus highly coupled. In this work we focus on the simultaneous control of the poloidal magnetic flux gradient  $z$  and the electron temperature  $T_e$ . These two parameters are modeled by nonlinear coupled resistive diffusion partial differential equations (PDEs).

Numerous results were obtained on designing control algorithms for the safety factor profile using Multi Input Multi Output (MIMO) lumped models [20], [2], [3], [22], [29]. A

simple control algorithm based on the singular value decomposition of the experimentally-deduced linear static response model for integrated control of  $q$  and  $T_e$  profiles is given in [18]. A control algorithm for simultaneous control of the  $q$  and  $T_e$  profiles, based on a MIMO approach for finite dimensional systems with a first principles model, is presented in [1].

In this paper we focus on developing control algorithms based on infinite dimensional control theory. Several works used this method to control the safety factor profile [4], [11], [13], with different levels of simplification regarding the impact of the temperature profile (through the plasma resistivity and the bootstrap currents). Nevertheless our work is the first, to the best of the authors' knowledge, to consider the stability and control of the coupled dynamics in the PDE framework. We consider diffusion coefficients that vary in space and time and extend the infinite dimensional Lyapunov analysis proposed by [4] to the system given by the two coupled PDEs for  $z$  and  $T_e$  profiles. We examine the stability of the nominal system and design a control strategy that improves the convergence rate to the desired equilibrium point.

Two control strategies are proposed: one based on a single control Lyapunov function for both variables and one that decouples the variables using singular perturbation theory. The first method is suitable for small tokamaks while the second is more suitable for large tokamaks, for which the difference between the time scales of the two states is larger. Singular perturbation theory is widely used in a control system theory [19], [17], [12]. Research works in boundary control of singularly perturbed partial differential equations with constant transport coefficients are introduced in [28], [27]. We propose a composite control strategy, where separate controls are calculated for the slow and fast dynamics of the system while taking into account the space variations of the coefficients.

The control methods developed in this paper are implemented on RAPTOR (RAPid Plasma Transport simulatOR) [9], a control-oriented, physics-based 1D code modeling the coupled  $q$  and  $T_e$  transport. The transport equations used in this simulator are nonlinear and tuned to match the data coming from real operating tokamaks [14]. The code is used as a tool for designing real time control applications, fast plasma simulation and as a real-time estimator running in parallel with the plasma discharge in TCV tokamak. Our control results are evaluated on the international thermonuclear experimental reactor (ITER) simulations using RAPTOR. ITER is the leading research tokamak that aims to prove the feasibility of using thermonuclear fusion for energy production.

The paper is organized as follows. In Section II the coupled

PDEs for  $z$  and  $T_e$  are presented and the control problem is defined. In Section III the simplified linearized model is derived. A Lyapunov function for stability analysis is computed for the linearized dynamics and used for convergence rate control in Section IV. In Section V the model is decoupled using singular perturbation theory and composite control is computed for the decoupled linearized system. The control implementation is presented in Section VI. In Section VII the results from the control implemented in the nonlinear RAPTOR simulator are presented. Due to space limitation some proofs and results are omitted. See [24] for a full version of this work.

## II. PROBLEM DESCRIPTION

### A. Magnetic flux dynamics

For control design we are interested in the evolution of the safety factor  $q = \frac{\partial \Phi}{\partial \Psi} = \frac{2\pi B_0 a^2 x}{\partial \Psi / \partial x}$  (or its reciprocal, the rotational transform  $\iota$ ), which is one of the key parameters to analyze the plasma stability and transport. The safety factor  $q$  denotes the ratio of toroidal to poloidal turns for a given magnetic field surface within a tokamak.  $\Psi$  is the poloidal magnetic flux,  $\Phi$  is toroidal magnetic flux,  $B_0$  the toroidal magnetic field at the center of the vacuum vessel and  $x = \rho/a$  is a normalized variable of the equivalent radius of the magnetic surfaces,  $\rho = \sqrt{\frac{\Phi}{\pi B_0}}$  and  $a$  being the small plasma radius.

We control  $q$  through the space derivative of the magnetic flux  $z = \frac{\partial \Psi}{\partial x}$ . To design a control law with real-time capabilities, we consider the simplified one-dimensional model for  $z$  (using the cylindrical approximation, which can be easily alleviated but simplifies the notations) as in [31]:

$$\frac{\partial z}{\partial t} = \frac{\partial}{\partial x} \left( \frac{\eta_{\parallel}}{\mu_0 a^2 x} \frac{\partial}{\partial x} (xz) \right) + \frac{\partial}{\partial x} (\eta_{\parallel} R_o j_{ni}) \quad (1)$$

with boundary conditions  $z(0, t) = 0$  and  $z(1, t) = -\frac{R_o \mu_0 I_p(t)}{2\pi}$ ,  $\forall t \geq 0$ , and initial condition  $z(x, 0) = z_0(x)$ ,  $\forall x \in [0, 1]$ .  $R_0$  is the major radius of the plasma (assumed constant in time),  $\mu_0$  is the permeability of vacuum and  $\eta_{\parallel}(x, t)$  is the parallel electrical resistivity of the plasma.  $I_p(t)$  is the total plasma current and  $j_{ni}(x, t)$  is the non-inductive current-density. The non-inductive current density is obtained by combining the auxiliary sources of current density  $j_{aux}(x, t)$  (current drive radio-frequency (RF) systems) and the bootstrap current density  $j_{bs}(x, t)$  as  $j_{ni} = j_{aux} + j_{bs}$ . The parameters  $\eta_{\parallel}(x, t)$  and  $j_{bs}(x, t)$  are highly dependent on the dynamics of the electron temperature  $T_e(x, t)$ . Simplified models for these parameters are given in [24].

### B. Electron temperature dynamics

The transport phenomena of the electrons temperature  $T_e$  and density  $n_e$  are coupled and modeled by a diffusion equation. This equation is obtained from simplified 1D energy transport and is presented as in [15], using the cylindrical approximation, as:

$$\frac{3}{2} \frac{\partial (n_e T_e)}{\partial t} = \frac{1}{a^2} \frac{1}{x} \frac{\partial}{\partial x} (x n_e \chi_e \frac{\partial T_e}{\partial x}) + Q_e \quad (2)$$

with boundary conditions  $\frac{\partial T_e}{\partial x}(0, t) = 0$  and  $T_e(1, t) = T_{e,edge}(t)$ ,  $\forall t \geq 0$ , and initial condition  $T_e(x, 0) = T_0(x)$ ,  $\forall x \in [0, 1]$ .  $\chi_e(x, t)$  is the electron diffusivity and  $Q_e(x, t)$  is the total electron heating power density. Note that  $\chi_e$  and  $Q_e$  depend on both  $z$  and  $T_e$ , rendering the system coupled and nonlinear. The net electron heating energy source  $Q_e$  results from several power densities:  $Q_e = Q_{OH} - Q_{ei} - Q_{rad} + Q_{aux}$  where  $Q_{OH}(x, t)$  is the ohmic effect,  $Q_{ei}(x, t)$  the electron-ion heat exchange,  $Q_{rad}(x, t)$  the radiation (their simplified models are given in [24]) and  $Q_{aux}(x, t)$  comes from the auxiliary sources.

Auxiliary actuators (such as neutral beam injection and RF antennas operated at ion cyclotron, electron cyclotron or lower hybrid frequencies) may act both on the current density  $j_{aux}(x, t)$  and on the power density  $Q_{aux}(x, t)$ , with a relative effect that depends on the nature of the actuator. The distributed controlled inputs  $j_{aux}(x, t)$  and  $Q_{aux}(x, t)$  thus depend on the same limited set of engineering variables  $u(t)$ , optimized to set the desired auxiliary profiles.

The goal of this work is to design a control strategy for the coupled dynamics of the inverse of the safety factor  $\iota$  (proportional to  $z$ ) and the electron temperature  $T_e$  using  $u(t)$ .

## III. LINEARIZED COUPLED DYNAMICS

For control purpose we linearize the model at a given equilibrium state  $(\bar{z}, \bar{T}_e)$  corresponding to the constant inputs  $\bar{u}$  and  $\bar{I}_p$ . An equilibrium is defined as a stationary solution of (1) and (2) as:

$$\begin{cases} 0 = \frac{\partial}{\partial x} \left( \frac{\bar{\eta}_{\parallel}}{\mu_0 a^2 x} \frac{\partial}{\partial x} (x\bar{z}) \right) + \frac{\partial}{\partial x} (\bar{\eta}_{\parallel} R_o \bar{j}_{ni}) \\ 0 = \frac{1}{a^2} \frac{1}{x} \frac{\partial}{\partial x} (x n_e \bar{\chi}_e \frac{\partial \bar{T}_e}{\partial x}) + \bar{Q}_e \end{cases} \quad (3)$$

The linearized model is derived around  $(\bar{z}, \bar{T}_e)$  by substituting, in the reference model from Section II,  $z = \bar{z} + \tilde{z}$ ,  $T_e = \bar{T}_e + \tilde{T}_e$ ,  $u = \bar{u} + \tilde{u}$  and  $I_p = \bar{I}_p + \tilde{I}_p$ , and using Taylor series with first order approximation.  $(\tilde{z}, \tilde{T}_e, \tilde{u}, \tilde{I}_p)$  thus denotes the variations around the equilibrium. The model is further simplified by considering the following assumptions:

- the electron density profile is constant during the heat process,  $n_e = n_e(x)$ ;
- the space variations of the electron density are neglected with respect to those of the temperature:  $\partial n_e / \partial x \ll \partial T_e / \partial x$ ;
- only the auxiliary heating/current drive systems are considered as controlled inputs, while  $I_p$  is assigned with a reference value,  $I_p(t) = \bar{I}_p$ . Note that  $I_p(t)$  could be used as a controlled input in our framework using the methods described in [7].

Under these assumptions, the simplified linearized coupled model coming from (1) and (2) is derived as:

$$\left\{ \begin{array}{l} \frac{\partial \tilde{z}}{\partial t} = \frac{\partial}{\partial x} \left( \frac{a_1(x)}{x} \frac{\partial}{\partial x} (x \tilde{z}) \right) + \frac{\partial}{\partial x} (a_2(x) \tilde{T}_e) \\ \quad + \frac{\partial}{\partial x} \left( a_3(x) \frac{\partial \tilde{T}_e}{\partial x} \right) + \frac{\partial}{\partial x} \left( a_4(x) \tilde{z} \right) \\ \quad + \frac{\partial}{\partial x} \left( a_5(x) \tilde{j}_{aux}(u, x, t) \right) \\ \varepsilon \frac{\partial \tilde{T}_e}{\partial t} = \frac{1}{x} \frac{\partial}{\partial x} \left( x b_1(x) \frac{\partial \tilde{T}_e}{\partial x} \right) - b_2(x) \tilde{T}_e \\ \quad + \frac{1}{x} \frac{\partial}{\partial x} \left( x b_3(x) \tilde{z} \right) + \frac{b_4(x)}{x} \left( \frac{\partial}{\partial x} (x \tilde{z}) \right) \\ \quad + b_5(x) \tilde{Q}_{aux}(u, x, t) \end{array} \right. \quad (4)$$

with boundary conditions,  $\forall t \geq 0$ :

$$\tilde{z}(0, t) = \tilde{z}(1, t) = \frac{\partial \tilde{T}_e}{\partial x}(0, t) = 0, \quad \tilde{T}_e(1, t) = \tilde{T}_{e,edge}(t) \quad (5)$$

and initial conditions:

$$\tilde{z}(x, t_0) = \tilde{z}_0; \quad \tilde{T}_e(x, t_0) = \tilde{T}_{e,0}, \quad \forall x \in [0, 1] \quad (6)$$

The coefficients of these PDEs  $a_i(x)$  and  $b_i(x)$  are given in [24].  $\varepsilon$  is the typical ratio between the energy confinement time and the characteristic resistive diffusion time, which varies with the size of the tokamak. In a small tokamak such as TCV  $\varepsilon \approx 0.07$  while in a large tokamak such as ITER this  $\varepsilon \approx 0.01$ . The relative time constants of the dynamics and the impact of the couplings between the states are thus very diverse.

#### IV. STABILITY ANALYSIS AND CONTROL OF THE COUPLED SYSTEM

##### A. Stability analysis

The stability of the coupled dynamics is analyzed with the following Lyapunov function candidate:

$$V(\tilde{z}, \tilde{T}_e) = \frac{1}{2} \int_0^1 \begin{bmatrix} \tilde{z} & \tilde{T}_e \end{bmatrix} \begin{bmatrix} x^2 p_1(x) & 0 \\ 0 & \gamma x^2 p_2(x) \end{bmatrix} \begin{bmatrix} \tilde{z} \\ \tilde{T}_e \end{bmatrix} dx \quad (7)$$

where  $p_1(x) > 0$  and  $p_2(x) > 0$  for  $x \in [0, 1]$  are polynomial functions. The candidate Lyapunov function is chosen as a weighted  $L^2(0, 1)$  norm and it is multiplied by the term  $x$  to handle the singularity at  $x = 0$ , which comes from the cylindrical representation of the system. The scaling parameter  $\gamma$  is added to balance the differences of amplitude between  $\tilde{z}$  and  $\tilde{T}_e$ . The stability of our coupled system of linearized equations is established with the following theorem.

**Theorem 1.** *Suppose that for a given positive number  $\alpha_1$  there exist polynomials  $p_1$  and  $p_2$  such that  $p_1(x) > 0$  and  $p_2(x) > 0$  for all  $x \in [0, 1]$ , and*

$$A_1(x) + \alpha_1 A_2(x) \leq 0 \quad (8)$$

for all  $x \in [0, 1]$ , where:

$$A_1(x) = \begin{bmatrix} A_{1,1}(x) & A_{1,2}(x) & A_{1,3}(x) & A_{1,4}(x) \\ A_{1,2}(x) & A_{2,2}(x) & A_{2,3}(x) & 0 \\ A_{1,3}(x) & A_{2,3}(x) & A_{3,3}(x) & A_{3,4}(x) \\ A_{1,4}(x) & 0 & A_{3,4}(x) & A_{4,4}(x) \end{bmatrix} \quad (9)$$

$$A_2(x) = \frac{1}{2} \begin{bmatrix} x^2 & 0 & 0 & 0 \\ 0 & \gamma x^2 & 0 & 0 \\ 0 & 0 & 0 & 0 \\ 0 & 0 & 0 & 0 \end{bmatrix} \quad (10)$$

and the elements in the  $A_1(x)$  matrix are given in (11) (see at the top of next page). Then the time derivative  $\dot{V}$  of  $V$  defined in (7) along the solutions of (4) and (5) verifies:

$$\begin{aligned} \dot{V} &\leq \frac{-\alpha_1}{\max_{x \in [0,1]} (p_1(x), p_2(x))} V \\ &\quad + \int_0^1 x^2 p_1(x) \frac{\partial}{\partial x} \left( a_4(x) \tilde{j}_{aux}(\tilde{u}, x, t) \right) \tilde{z} dx \\ &\quad + \gamma \int_0^1 \frac{x^2 p_2(x)}{\varepsilon} b_5(x) \tilde{Q}_{aux}(\tilde{u}, x, t) \tilde{T}_e dx, \quad \forall t \geq 0 \end{aligned} \quad (12)$$

*Proof.* See [24].  $\square$

The nominal stability ( $\tilde{u} = 0$ ) is then directly obtained with the following corollary.

**Corollary 1.** *If the conditions of Theorem 1 are satisfied, the system (4) with  $\tilde{u} = 0$ , boundary conditions (5) and initial conditions (6) is globally exponentially stable. The convergence rate of the system satisfies  $V(t) \leq e^{-\beta_1 t} V(\tilde{z}_0, \tilde{T}_{e,0})$ , where  $\beta_1 = -\alpha_1 / [\max_{x \in [0,1]} (p_1(x), p_2(x))]$ .*

*Proof.* This result is directly obtained by setting  $\tilde{u} = 0$ : the variations of the auxiliary current and power density are zero ( $\tilde{j}_{aux} = \tilde{Q}_{aux} = 0$ ) and from Theorem 1 we obtain the inequality  $\dot{V} \leq -\beta_1 V$ ,  $\forall t \geq 0$ . Integrating this inequality over time implies the desired inequality on  $V(t)$ .  $\square$

##### B. Calculation of the Lyapunov Function

Using Legendre polynomials for  $p_1$  and  $p_2$  the inequality (8) is formulated and solved as an LMI problem defined with  $x$  in the range  $[0, 1]$ . Legendre polynomials are orthogonal in the range  $[-1, 1]$ , and the polynomials  $p_1$  and  $p_2$  can be expanded in this interval in terms of them as [16]:

$$p_1(x) = \sum_{i=0}^{N_1} c_{1,i} P_i(x), \quad p_2(x) = \sum_{i=0}^{N_2} c_{2,i} P_i(x)$$

where  $c_{1,1}, \dots, c_{1,N_1}$  and  $c_{2,1}, \dots, c_{2,N_2}$  are some constant coefficients,  $P_i(x)$  is the  $i^{th}$  order Legendre polynomial, and  $N_1$  and  $N_2$  are the orders of the Legendre polynomials for  $p_1$  and  $p_2$ , respectively.

Sampling the interval  $[0, 1]$  and representing  $p_1$  and  $p_2$  as a sum of Legendre polynomials permit us to formulate the following LMI problem:

$$\text{Maximize } \alpha_1 \geq 0$$

such that the polynomials  $p_1(x)$  and  $p_2(x)$  satisfy, for all  $x \in [0, 1]$ ,

- 1)  $0 < p_1(x) \leq p_{1,max}$  and  $0 < p_2(x) \leq p_{2,max}$ ;
- 2)  $A_1(x) + \alpha_1 A_2(x) \leq 0$ .

This LMI problem for finding the unknown constant parameters  $c_{1,1}, \dots, c_{1,N_1}$  and  $c_{2,1}, \dots, c_{2,N_2}$  is solved using YALMIP toolbox [21] for MATLAB  $\text{\textcircled{R}}$ .

$$\begin{aligned}
A_{1,1} &= \frac{1}{2} \left( 3xp_1'(x) + x^2p_1''(x) - p_1(x) \right) a_1(x) + \frac{1}{2} a_1'(x) \left( x^2p_1'(x) + 3xp_1(x) \right) - 2xp_1(x)a_4(x) - x^2p_1'(x)a_4(x) \\
A_{1,2} &= -xp_1(x)a_2(x) - \frac{1}{2}x^2p_1'(x)a_2(x) + \frac{\gamma}{2\varepsilon}xb_3(x) \left( xp_2'(x) + p_2(x) \right) + \frac{\gamma}{2\varepsilon}xp_2(x)b_4(x) \\
A_{1,3} &= -\frac{1}{2}x^2p_1(x)a_4(x), \quad A_{1,4} = -xp_1(x)a_3(x) - \frac{1}{2}x^2p_1'(x)a_3(x) \\
A_{2,2} &= -\frac{\gamma}{\varepsilon}x^2p_2(x)b_2(x) + \frac{\gamma}{2\varepsilon}b_1(x) \left( x^2p_2''(x) + 2xp_2'(x) + p_2(x) \right) + \frac{\gamma}{2\varepsilon}b_1'(x) \left( x^2p_2'(x) + xp_2(x) \right) \\
A_{2,3} &= -\frac{1}{2}x^2p_1(x)a_2(x) - \frac{\gamma}{2\varepsilon}x^2b_3(x)p_2(x) + \frac{\gamma}{2\varepsilon}x^2p_2(x)b_4(x) \\
A_{3,3} &= -x^2p_1(x)a_1(x), \quad A_{3,4} = -\frac{1}{2}x^2p_1(x)a_4(x), \quad A_{4,4} = -\frac{\gamma}{\varepsilon}x^2b_1(x)p_2(x)
\end{aligned} \tag{11}$$

### C. Convergence rate control

Considering the results of Theorem 1, a control strategy can be defined to accelerate the convergence rate of the system. This is done with the following corollary.

**Corollary 2.** *If the conditions of Theorem 1 are verified, the feedback control parameters  $\tilde{u}$  can be calculated to obtain the following equality:*

$$\begin{aligned}
&\int_0^1 x^2p_1(x) \frac{\partial}{\partial x} \left( a_4(x) \tilde{j}_{aux}(\tilde{u}, x, t) \right) \tilde{z} dx \\
&+ \gamma \int_0^1 \frac{x^2p_2(x)}{\varepsilon} b_5(x) \tilde{Q}_{aux}(\tilde{u}, x, t) \tilde{T}_e dx = -\alpha_2 V
\end{aligned} \tag{13}$$

where  $\alpha_2 > 0$  is a tuning parameter. Using this feedback control, the system (4) with boundary conditions (5) is globally exponentially stable and the convergence rate of the Lyapunov function satisfies  $\dot{V} \leq -\beta_2 V$ , where  $\beta_2 = (\alpha_1 + \alpha_2) / [\max_{x \in [0,1]} (p_1(x), p_2(x))]$ .

The convergence rate is thus increased by a factor  $\alpha_2 / [\max_{x \in [0,1]} (p_1(x), p_2(x))]$  by designing a control law that solves (implicitly) equation (13) for  $\tilde{u}$ .

Note that this controller is suitable for systems with commensurate time scales, such as small scale tokamaks, but is not effective enough to improve the convergence rate of a system with different time scales [19]. The control strategy for large tokamaks is discussed in the next section.

## V. SYSTEM DECOUPLING USING SINGULAR PERTURBATION THEORY

In large tokamaks, the dynamics of  $z$  is much slower than the dynamics of  $T_e$  [25]. The system of PDEs (4)-(6) can thus be divided into two different time scales by introducing the fast time scale  $\tau = \varepsilon t$ . Singular perturbation theory is applied by isolating the slow variables, which are considered as fixed in the fast time scale and solved using static equations (thus separated from the fast component).

Considering that  $\varepsilon \ll 1$ , the electrons temperature dynamics can be decomposed into two components: the slow component  $\tilde{T}_s$  that evolves with the (slow) variations of the magnetic flux and the fast component  $\tilde{T}_f$  that reacts more rapidly to inputs variation. We thus have  $\tilde{T}_e = \tilde{T}_s + \tilde{T}_f$ . At the slow time scale,

the static equation for the electron temperature is computed using the assumption that  $\partial \tilde{T}_s / \partial \tau \ll \partial \tilde{T}_f / \partial \tau$  in the heat equation. In this equation  $\tilde{T}_e$  is replaced by  $\tilde{T}_s$ , which denotes the slow variation of the temperature.  $\tilde{T}_s$  is called the quasi-steady state (QSS) and is determined by:

$$\begin{aligned}
0 &= \frac{1}{x} \frac{\partial}{\partial x} \left( xb_1(x) \frac{\partial \tilde{T}_s}{\partial x} \right) - b_2(x) \tilde{T}_s + \frac{1}{x} \frac{\partial}{\partial x} (xb_3(x) \tilde{z}) \\
&+ \frac{b_4(x)}{x} \left( \frac{\partial}{\partial x} (x\tilde{z}) \right) + b_5(x) \tilde{Q}_{aux,s}(\tilde{u}_s, x, t)
\end{aligned} \tag{14}$$

where  $\tilde{u}_s$  is the slow component of the input and with boundary conditions  $\frac{\partial \tilde{T}_s}{\partial x}(0, t) = 0$  and  $\tilde{T}_s(1, t) = \tilde{T}_{e,edge}(t)$ . The solution of  $\tilde{T}_s(x, t)$  is calculated at each time instant from  $\tilde{z}$  and  $\tilde{u}_s$  in (14) using numerical methods. The evolution of the fast dynamics is included with a boundary layer model, obtained in the fast time scale as:

$$\begin{aligned}
\frac{\partial \tilde{T}_f}{\partial \tau} &= \frac{1}{x} \frac{\partial}{\partial x} \left( xb_1(x) \frac{\partial \tilde{T}_f}{\partial x} \right) - b_2(x) \tilde{T}_f \\
&+ b_5(x) \tilde{Q}_{aux,f}(\tilde{u}_f, x, \tau)
\end{aligned} \tag{15}$$

with boundary conditions:

$$\frac{\partial \tilde{T}_f}{\partial x}(0, \tau) = 0; \quad \tilde{T}_f(1, \tau) = 0 \tag{16}$$

where  $\tilde{u}_f$  stands for the fast component of the input.

The magnetic field component  $\tilde{z}$  writes in terms of  $\tilde{T}_s$  as:

$$\begin{aligned}
\frac{\partial \tilde{z}}{\partial t} &= \frac{\partial}{\partial x} \left( \frac{a_1(x)}{x} \frac{\partial}{\partial x} (x\tilde{z}) \right) + \frac{\partial}{\partial x} (a_2(x) \tilde{T}_s) \\
&+ \frac{\partial}{\partial x} \left( a_3(x) \frac{\partial \tilde{T}_s}{\partial x} \right) + \frac{\partial}{\partial x} (a_4(x) \tilde{z}) \\
&+ \frac{\partial}{\partial x} \left( a_5(x) \tilde{j}_{aux}(u_s, x, t) \right)
\end{aligned} \tag{17}$$

with boundary conditions:

$$\tilde{z}(0, t) = 0; \quad \tilde{z}(1, t) = 0 \tag{18}$$

Our dynamics is thus composed of two PDEs at evolving at different time scales, (15) and (17) with their boundary and initial conditions, and one PDE that acts as an algebraic constraint (14) with its boundary conditions. The composite control is obtained by separately calculating and combining the slow and the fast components as  $\tilde{u} = \tilde{u}_s + \tilde{u}_f$ .

### A. Slow component stability and control

The slow component of the control is calculated by considering only the magnetic flux dynamics (17) and the following Lyapunov function candidate is chosen:

$$V_s(\tilde{z}) = \frac{1}{2} \int_0^1 x^2 p_s(x) \tilde{z}^2 dx \quad (19)$$

The evolution of this Lyapunov function is inferred from the following theorem.

**Theorem 2.** *Suppose that for a given positive number  $\alpha_3$  there exists a polynomial  $p_s$  such that  $p_s(x) > 0$  for all  $x \in [0, 1]$  and satisfying, for all  $x \in [0, 1]$ ,*

$$\begin{aligned} & \frac{a_1(x)}{2} \left( 3xp'_s(x) + x^2 p''_s(x) - p_s(x) \right) \\ & + \frac{a'_1(x)}{2} \left( x^2 p'_s(x) + 3xp_s(x) \right) + \frac{x^2}{2} a'_4(x) p_1(x) \quad (20) \\ & + a_4(x) \left( xp_s(x) + \frac{x^2}{2} p'_1(x) \right) \leq -\frac{\alpha_3}{2} x^2 \end{aligned}$$

Then the time derivative  $\dot{V}_s$  of the function  $V_s$  defined by (19) verifies:

$$\begin{aligned} \dot{V}_s \leq & -\beta_3 V_s + \int_0^1 x^2 p_s(x) \frac{\partial}{\partial x} \left( a_2(x) \tilde{T}_s + a_3(x) \frac{\partial \tilde{T}_s}{\partial x} \right) \tilde{z} dx \\ & + \int_0^1 x^2 p_s(x) \frac{\partial}{\partial x} \left( a_5(x) \tilde{j}_{aux}(\tilde{u}_s, x, t) \right) \tilde{z} dx \quad (21) \end{aligned}$$

where  $\beta_3 = \frac{\alpha_3}{\max_{x \in [0,1]} p_s(x)}$

*Proof.* See [24].  $\square$

We use the dynamics (21) to design a convergence rate controller, as described in the following corollary.

**Corollary 3.** *If the conditions of Theorem 2 are verified, the feedback control parameters of the slow component  $\tilde{u}_s$  can be calculated to obtain the following relation:*

$$\begin{aligned} & \int_0^1 x^2 p_s(x) \frac{\partial}{\partial x} \left( a_2(x) \tilde{T}_s + a_3(x) \frac{\partial \tilde{T}_s}{\partial x} \right) \tilde{z} dx \\ & + \int_0^1 x^2 p_s(x) \frac{\partial}{\partial x} \left( a_5(x) \tilde{j}_{aux}(\tilde{u}_s, x, t) \right) \tilde{z} dx = -\alpha_4 V_s \quad (22) \end{aligned}$$

where  $\alpha_4 > 0$  is a tuning parameter. Using this feedback control, the system (17) with boundary conditions (18) is globally exponentially stable with a convergence rate that satisfies  $\dot{V}_s \leq -\beta_4 V_s$ , where  $\beta_4 = \frac{\alpha_3 + \alpha_4}{\max_{x \in [0,1]} p_s(x)}$ .

### B. Fast component stability and control

The fast component of the system has dynamics governed by (15)-(16). To compute the stability of this system (boundary layer system), the following candidate Lyapunov function is selected:

$$V_f(\tilde{T}_f) = \frac{1}{2} \int_0^1 p_f(x) \tilde{T}_f^2 dx \quad (23)$$

and its dynamics is studied in the following theorem.

**Theorem 3.** *Suppose that for a given positive number  $\alpha_5$  there exists a polynomial  $p_f$  such that  $p_f(x) > 0$  for all  $x \in [0, 1]$  and satisfying, for all  $x \in [0, 1]$ ,*

$$\begin{aligned} & \frac{b_1(x)}{2} \left( x^2 p''_f(x) + 2xp'_f(x) + p_f(x) \right) \\ & + \frac{b'_1(x)}{2} \left( x^2 p'_f(x) + xp_f(x) \right) - x^2 b_2(x) p_f(x) \leq -\frac{\alpha_5}{2} x^2 \quad (24) \end{aligned}$$

Then the time derivative  $\dot{V}_f$  of the function  $V_f$  defined by (23) verifies:

$$\dot{V}_f \leq -\beta_5 V_f + \int_0^1 x^2 p_f(x) b_5(x) \tilde{Q}_{aux,f}(\tilde{u}_f, x, \tau) \tilde{T}_f dx \quad (25)$$

where  $\beta_5 = \frac{\alpha_5}{\max_{x \in [0,1]} p_f(x)}$ .

*Proof.* See [24].  $\square$

The convergence rate of the boundary layer system is controlled using the following corollary.

**Corollary 4.** *If the conditions of Theorem 3 are verified, the feedback control parameters of the boundary layer system  $\tilde{u}_f$  can be calculated to obtain the following relation:*

$$\int_0^1 x^2 p_f(x) b_5(x) \tilde{Q}_{aux,f}(\tilde{u}_f, x, \tau) \tilde{T}_f dx = -\alpha_6 V_f \quad (26)$$

where  $\alpha_6 > 0$  is a tuning parameter. Using this feedback control, the system (15) with boundary conditions (16) is globally exponentially stable with a convergence rate that satisfies  $\dot{V} \leq -\beta_6 V$ , where  $\beta_6 = \frac{\alpha_5 + \alpha_6}{\max_{x \in [0,1]} p_f(x)}$ .

Numerical algorithms to solve the functional equation (20) to find  $p_s$  from Theorem 2 and the functional equation (24) for  $p_f$  from Theorem 3 can be found in [4], [5]. In this work, these inequalities are scalar and they are found using Legendre polynomials and the algorithm solving the LMI problem, as the one defined in Section IV-B.

## VI. CONTROL IMPLEMENTATION

### A. Auxiliary current and power density models

The auxiliary sources are modeled as simple weighted Gaussian distributions as proposed in [31], with the analytical parametrization defined for RAPTOR in [10]. These distributions approximate both the power and current densities. The total auxiliary current density is computed as the sum of the current densities induced by each electron cyclotron (EC) antenna:

$$j_{aux} = \sum_{i=1}^{n_{aux}} \frac{\bar{T}_e}{n_e} j_{dis,i}(x) P_{aux,i}(t) \quad (27)$$

where  $n_{aux}$  denotes the number of the auxiliary sources and  $j_{dis,i}(x)$  is a weighted Gaussian distribution (given in [10]), representing the normalized reference current density profile

generated by the input powers  $P_{aux,i}(t)$  and the current-drive efficiency  $(\frac{\tilde{T}_e}{n_e})$ .

Similarly, the total auxiliary power density is composed by the sum of the individuals induced by each EC antenna:

$$Q_{aux} = \sum_{i=1}^{n_{aux}} Q_{dis,i}(x) P_{aux,i}(t) \quad (28)$$

where  $Q_{dis,i}(x)$  (given in [10]) is a normalized reference power density deposition profile for the  $i$ -th auxiliary source. In our control application,  $Q_{dis,i}(x)$  and  $j_{dis,i}(x)$  are fixed by the choice of the position and distribution of the EC antennas. Only the input powers  $P_{aux,i}(t)$  are thus available to achieve the desired control signals and  $u(t) = [P_{aux,1}(t), \dots, P_{aux,n_{aux}}(t)]$ .

### B. Calculation of the control inputs

The control is implemented using only a limited number of actuators (the powers of the EC clusters  $P_{aux,i}(t)$ ) while our convergence rate controllers imply the evolution of full spatial distributions. An extra step is thus needed to optimize the engineering parameters according to the control objective. This is achieved by solving (e.g. for Corollary 2) the following optimization problem at each time instant:

$$\begin{aligned} \min_{\tilde{u}} J(\tilde{u}) \\ \text{subject to : } -\alpha_2 V \leq J(\tilde{u}) \leq 0 \\ \tilde{u}_{min} \leq \tilde{u} \leq \tilde{u}_{max} \end{aligned} \quad (29)$$

with

$$\begin{aligned} J(\tilde{u}) = \int_0^1 x^2 p_1(x) \frac{\partial}{\partial x} (a_4(x) \tilde{j}_{aux}(\tilde{u}, x)) \tilde{z} dx \\ + \int_0^1 x^2 \frac{\gamma p_2(x)}{\epsilon} b_5(x) \tilde{Q}_{aux}(\tilde{u}, x) \tilde{T}_e dx \end{aligned}$$

where  $\tilde{u}_{min}$  and  $\tilde{u}_{max}$  stand for the minimum and maximum values of the allowed power for each antenna.

**Remark.** *The convergence rate of the system in this section is calculated from a practical implementation standpoint. It takes into account the limitations of the current and of the power distribution profiles, imposed by the limitations of the auxiliary heating sources. These limitations make the equality (13) to be very restrictive and difficult to achieve. The optimization (29) solves the optimal engineering parameters to reach the desired convergence rate  $\alpha_2$  in a less strict way. Therefore, the closed-loop system is stable and the convergence rate varies in the range:  $-\beta_1 V \leq \dot{V} \leq -\beta_2 V$  (between the open-loop and unconstrained control values), depending on the actuators limitations.*

The decoupling control implies two objective functions: one for the slow (22) and one for the fast component (26). Combining these two functions for feedback control design, the following multi-objective optimization problem is formulated:

$$\begin{aligned} \min_{\tilde{u}=\tilde{u}_s+\tilde{u}_f} \omega_1 J_s(\tilde{u}_s) + \omega_2 J_f(\tilde{u}_f) \\ \text{subject to : } -\alpha_4 \mathcal{V}_s \leq J_s(\tilde{u}_s) \leq 0 \\ -\alpha_6 \mathcal{V}_f \leq J_f(\tilde{u}_f) \leq 0 \\ \tilde{u}_{min} \leq \tilde{u}_s + \tilde{u}_f \leq \tilde{u}_{max} \end{aligned} \quad (30)$$

with

$$\begin{aligned} J_s(\tilde{u}_s) = \int_0^1 x^2 p_s(x) \frac{\partial}{\partial x} \left( a_2(x) \tilde{T}_s + a_3(x) \frac{\partial \tilde{T}_s}{\partial x} \right) \tilde{z} dx \\ + \int_0^1 x^2 p_s(x) \frac{\partial}{\partial x} \left( a_5(x) \tilde{j}_{aux}(\tilde{u}_s, x) \right) \tilde{z} dx \\ J_f(\tilde{u}_f) = \int_0^1 x^2 p_f(x) b_5(x) \tilde{Q}_{aux,f}(\tilde{u}_f, x) \tilde{T}_f dx \end{aligned}$$

The weights  $\omega_1, \omega_2 > 0$  are tuning parameters and  $\tilde{T}_s$  is found as the solution of (14) at each time instant using  $\tilde{z}$  and  $\tilde{u}_s$ .

## VII. RESULTS

The two control strategies presented in the previous sections are evaluated using the nonlinear tokamak simulator RAPTOR. While real tokamak experiments for feedback control purposes are particularly difficult to obtain, RAPTOR provides a valid alternative as it includes the main physical properties of the plasma at the time scales of our study and has been successfully compared with experimental measurements on numerous test cases. Furthermore, RAPTOR can be runned outside of the control environment as a simulator in stand-alone situation as well as being used as an estimator for the control algorithms implemented in the actual tokamak control system, when implemented. Using RAPTOR as a reference simulator is thus particularly relevant for control design evaluation [10], [9], [1], [14], [22], [29]. We chose to focus the simulation results on the impact of the different time scales only, due to space limitations. Analysis and simulation results related to robustness and to the impact of extra additional heatings can be found in [7], [6], [23].

Our control approaches are evaluated and compared on the tokamak configuration of ITER ( $\epsilon \approx 0.01$ ) in L-mode, emphasizing the interest for considering the different time scales separately for large tokamaks. Three EC antennas are used as actuators. The plasma current is set to a constant  $I_p = 7$  MA and a linearized model is obtained by extracting the parameters corresponding to a stationary state when constant values of the powers of the EC antennas are  $P_{ec1} = P_{ec2} = P_{ec3} = 7$  MW. The input powers are limited in the range of 0 to 10 MW. Several reference profiles are obtained to test the controllers performance. An additional EC antenna is introduced to test the robustness with respect to deviations from the calculated equilibrium point.

Since both control methods ask for a choice concerning the relative importance of the magnetic flux control with respect to the electrons heat control, we consider two control cases: Case 1 emphasizes the convergence rate of  $\tilde{z}$  while  $\tilde{T}_e$  is the priority for Case 2. Both control methods are evaluated on each case.

We first implement the coupled control presented in Section IV. The convergence rate is set by the tuning parameter  $\alpha_1$  and the nature of the response depends highly on the choice of the scaling parameter  $\gamma$  (which multiplies  $\tilde{T}_e$  in the Lyapunov function (7)). When  $\gamma$  is low (Case 1), the control is more effective for the performance of the slow variable  $\tilde{z}$  while the convergence rate of  $T_e$  is difficult to tune (typically enduring high overshoots). When the value of  $\gamma$  is high (Case 2), the

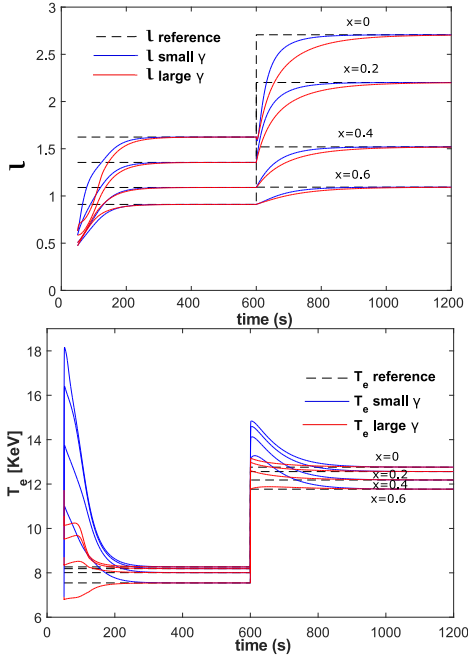


Fig. 1: Evolution  $\iota$  (top) and  $T_e$  (bottom) in the ITER simulation with the coupled controller and with convergence priority given to  $\tilde{z}$  (Case 1, small  $\gamma$ ) or  $\tilde{T}_e$  (Case 2, large  $\gamma$ ).

performance of the convergence rate of  $T_e$  can be tuned but the convergence rate of  $\tilde{z}$  is free. To improve the convergence rate of  $\tilde{z}$  we need in this case to increase the value of  $\alpha_1$ , which induces oscillations in the  $T_e$  profile. The results from these simulations are presented in Fig. 1. While the convergence of  $\iota$  and  $T_e$  is achieved in both control cases, the disparity in the convergence rates of the two dynamics renders the relative tuning particularly difficult to achieve, motivating the system decoupling approach.

We now apply the composite control presented in Section V. The polynomials of the Lyapunov functions, presented in Fig. 3, are computed separately for the fast and the slow components. The maximum values of the convergence rate parameters are calculated numerically as  $\alpha_4 = 0.01$  and  $\alpha_7 = 9.3$ . The difference between these two values was expected due to the difference in the time scales. The solution of the slow component of the temperature (14) is numerically calculated at each time instant and subtracted from  $\tilde{T}_e$  to estimate the fast component of the temperature  $\tilde{T}_f$ . The output parameters  $\iota(x, t)$  and  $T_e(x, t)$  at several locations are presented in Fig. 2 for the two control cases. For Case 1 a feedback control is applied only on the slow component of the system. The results from this simulation have similar performance as in the case when the method presented in Section IV is applied and low  $\gamma$  is used. For Case 2 the composite control combines the feedback control of the fast and slow components. The effect of the feedback control on the boundary layer system can be observed on  $T_e(x, t)$ : applying a control on the boundary layer system results in a reduced overshoot and a better convergence of the fast component at the cost of a slower convergence of the slow component. This behavior is also observed on the time-evolution of the Lyapunov function in Cases 1 and

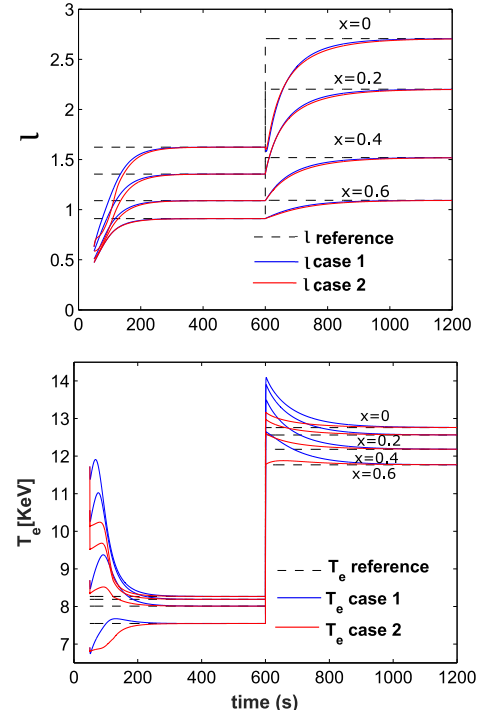


Fig. 2: Evolution of  $T_e$  and  $\iota$  in the ITER simulation with composite control for Case 1 and Case 2.

2 starting from  $t = 600s$  (when the reference profiles are changed) in Fig. 4.

The tuning of the closed-loop performance with the composite control can be done by changing the values of the weighting parameters  $\omega_{1,2}$  to obtain the desired balance between the two components. The convergence rate of the closed-loop system is selected by the choice of  $\alpha_4$  and  $\alpha_6$  for the performance of the slow and fast component, respectively. Increasing the value of  $\alpha_4$  decreases the settling time and decreases the steady state error of the slow component, but increases the overshoot of the electron temperature. By increasing the value of  $\alpha_6$  the convergence rate of the fast component is improved and the overshoot of the electron temperature is decreased. If  $\alpha_6$  is increased further, it leads to high oscillations of the fast varying component. Note also that when the two control functions are calculated separately we can apply different sampling periods for the two parameters, which improves the computational efficiency and the performance of the feedback control.

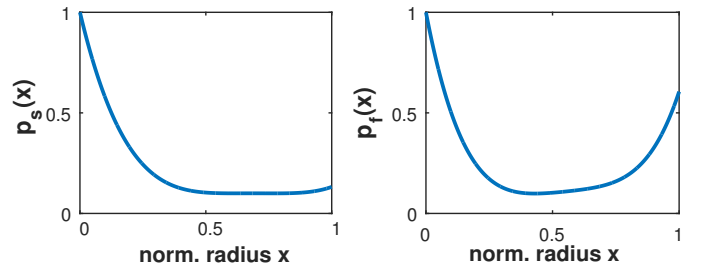


Fig. 3: Numerical solution of the composite control polynomials  $p_s$  and  $p_f$  for ITER.

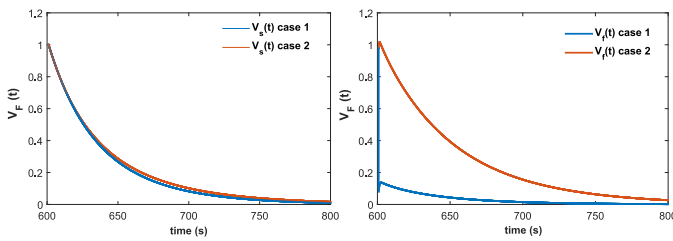


Fig. 4: Time-evolution of the two normalized Lyapunov functions of the composite control ( $V_s$  and  $V_f$ ) for the ITER simulation.

## VIII. CONCLUSIONS AND FUTURE WORK

Integrated feedback control algorithms for coupled current and electron temperature profiles in tokamaks are developed and tested in this work. The plasma states are modeled as two coupled inhomogeneous 1D diffusion PDEs and a control-oriented model is proposed using linearized simple models for the controlled plasma parameters. The control design is based on the infinite dimensional settings by using control Lyapunov functions. Our first control method is based on the coupled dynamics and on a single Lyapunov function. The different time scales of the two states motivated a second control strategy designed by decoupling the two time scales of the system using singular perturbation theory. Both controllers are evaluated using the nonlinear RAPTOR tokamak plasma simulator, parametrized for ITER. The different times scales permit us to compare the two control strategies. In the future, our control strategies can be used in a real tokamak machine using the state observer for the plasma profiles developed in [8]. A future perspective is also to consider the ohmic heating sources in the control design, as a boundary input.

## ACKNOWLEDGMENTS

The authors would like to thank Federico Felici for invaluable help in the use of RAPTOR. This work has been partially supported by the ANR project TORID contract number ANR-12-BS03-0008.

## REFERENCES

- [1] J. E. Barton, W. P. Wehner, E. Schuster, F. Felici, and O. Sauter. Simultaneous closed-loop control of the current profile and the electron temperature profile in the TCV tokamak. In *American Control Conference*, pages 3316–3321, Chicago, USA, 2015.
- [2] M. D. Boyer, J. Barton, E. Schuster, T. C. Luce, J. R. Ferron, M. L. Walker, D. A. Humphreys, B. G. Penaflor, and R. D. Johnson. First-principles-driven model-based current profile control for the DIII-D tokamak via LQI optimal control. *Plasma Physics and Controlled Fusion*, 55(10):105007, 2013.
- [3] M. D. Boyer, J. Barton, E. Schuster, M. L. Walker, T. C. Luce, J. R. Ferron, B. G. Penaflor, R. D. Johnson, and D. A. Humphreys. Backstepping control of the toroidal plasma current profile in the DIII-D tokamak. *IEEE Trans. on Control Systems Technology*, 22(5):1725–1739, 2014.
- [4] F. Bribiesca Argomedo, C. Prieur, E. Witrant, and S. Brémond. A strict control Lyapunov function for a diffusion equation with time-varying distributed coefficients. *IEEE Trans. on Automatic Control*, 58(2):290–303, 2013.
- [5] F. Bribiesca Argomedo, E. Witrant, and C. Prieur. D 1-Input-to-state stability of a time-varying nonhomogeneous diffusive equation subject to boundary disturbances. In *American Control Conference*, pages 2978–2983, Montreal, Canada, 2012.
- [6] F. Bribiesca Argomedo, E. Witrant, and C. Prieur. *Safety Factor Profile Control in a Tokamak*. Springer, 2014.
- [7] F. Bribiesca Argomedo, E. Witrant, C. Prieur, S. Brémond, R. Nouailletas, and J. F. Artaud. Lyapunov-based distributed control of the safety factor profile in a tokamak plasma. *Nuclear Fusion*, 53(3):033005, 2013.
- [8] F. Felici, M. de Baar, and M. Steinbuch. A dynamic state observer for real-time reconstruction of the tokamak plasma profile state and disturbances. In *American Control Conference*, pages 4816–4823, Portland, USA, 2014.
- [9] F. Felici and O. Sauter. Non-linear model-based optimization of actuator trajectories for tokamak plasma profile control. *Plasma Physics and Controlled Fusion*, 54(2):025002, 2012.
- [10] F. Felici, O. Sauter, S. Coda, B. Duval, T. Goodman, J. Moret, J. Paley, T. Team, et al. Real-time physics-model-based simulation of the current density profile in tokamak plasmas. *Nuclear Fusion*, 51(8):083052, 2011.
- [11] A. Gahlawat, E. Witrant, M. M. Peet, and M. Alamir. Bootstrap current optimization in tokamaks using sum-of-squares polynomials. In *51st Annual Conference on Decision and Control*, pages 4359–4365, 2012.
- [12] Z. Gajic. *Optimal control of singularly perturbed linear systems and applications*. CRC Press, 2001.
- [13] O. Gaye, L. Autrique, Y. Orlov, E. Moulay, S. Brémond, and R. Nouailletas.  $H_\infty$  stabilization of the current profile in tokamak plasmas via an LMI approach. *Automatica*, 49(9):2795–2804, 2013.
- [14] P. Geelen, F. Felici, A. Merle, and O. Sauter. Parameter estimation for a nonlinear control-oriented tokamak profile evolution model. *Plasma Physics and Controlled Fusion*, 57(12):125008, 2015.
- [15] F. Hinton and R. Hazeltine. Theory of plasma transport in toroidal confinement systems. *Reviews of Modern Physics*, 48(2):239, 1976.
- [16] W. Kaplan. *Advanced calculus*. Addison Wesley, 2002.
- [17] H. K. Khalil. *Nonlinear systems*. Prentice Hall, Upper Saddle River, (N.J.), 3rd edition, 2002.
- [18] S. Kim and J. Lister. A potentially robust plasma profile control approach for iter using real-time estimation of linearized profile response models. *Nuclear Fusion*, 52(7):074002, 2012.
- [19] P. Kokotovic, H. K. Khalil, and J. O’reilly. *Singular perturbation methods in control: analysis and design*, volume 25. SIAM, 1999.
- [20] L. Laborde, D. Mazon, D. Moreau, A. Murari, R. Felton, L. Zabeo, R. Albanese, M. Ariola, J. Bucalossi, F. Crisanti, et al. A model-based technique for integrated real-time profile control in the JET tokamak. *Plasma Physics and Controlled Fusion*, 47(1):155, 2005.
- [21] J. Löfberg. YALMIP: A toolbox for modeling and optimization in matlab. In *IEEE International Symposium on Computer Aided Control Systems Design*, pages 284–289, Taipei, Taiwan, 2004.
- [22] E. Maljaars, F. Felici, M. De Baar, J. van Dongen, G. Hogewei, P. Geelen, and M. Steinbuch. Control of the tokamak safety factor profile with time-varying constraints using mpc. *Nuclear Fusion*, 55(2):023001, 2015.
- [23] B. Mavkov. *Control of Coupled Transport in Tokamak Plasmas*. PhD thesis, Université Grenoble Alpes, 2017.
- [24] B. Mavkov, E. Witrant, and C. Prieur. Distributed control of coupled inhomogeneous diffusion in tokamak plasmas (full version). 2017.
- [25] D. Moreau, D. Mazon, M. Ariola, G. De Tommasi, L. Laborde, F. Piccolo, F. Sartori, T. Tala, L. Zabeo, A. Boboc, et al. A two-time-scale dynamic-model approach for magnetic and kinetic profile control in advanced tokamak scenarios on JET. *Nuclear Fusion*, 48(10):106001, 2008.
- [26] A. Pironti and M. Walker. Fusion, tokamaks, and plasma control: an introduction and tutorial. *IEEE Control System Magazine*, 25(5):30–43, 2005.
- [27] Y. Tang, C. Prieur, and A. Girard. Tikhonov theorem for linear hyperbolic systems. *Automatica*, 57:1–10, 2015.
- [28] R. Vazquez and M. Krstic. *Control of turbulent and magnetohydrodynamic channel flows: boundary stabilization and state estimation*. Springer Science & Business Media, 2008.
- [29] N. M. T. Vu, R. Nouailletas, L. Lefèvre, and F. Felici. Plasma q-profile control in tokamaks using a damping assignment passivity-based approach. *Control Engineering Practice*, 54:34–45, 2016.
- [30] J. Wesson. *Tokamaks*, volume 149 of *International Series of Monographs on Physics*. Oxford University Press, Oxford, UK, 4<sup>th</sup> edition, 2011.
- [31] E. Witrant, E. Joffrin, S. Brémond, G. Giruzzi, D. Mazon, O. Barana, and P. Moreau. A control-oriented model of the current profile in tokamak plasma. *Plasma Physics and Controlled Fusion*, 49(7):1075, 2007.